Supplementary Information

Deformability-induced lift force in spiral microchannels for cell separation

Ewa Guzniczak[1]*, Oliver Otto[2], Graeme Whyte[1], Nicholas Willoughby[1], Melanie Jimenez[3] & Helen Bridle[1]

[1]Heriot-Watt University, School of Engineering and Physical Science, Department of Biological Chemistry, Biophysics and Bioengineering Edinburgh Campus, Edinburgh, EH14 4AS, Scotland

[2] Centre for Innovation Competence – Humoral Immune Reactions in Cardiovascular Diseases, University of Greifswald, Fleischmannstr. 42, 17489 Greifswald, Germany

and:

Deutsches Zentrum für Herz-Kreislaufforschung, Partner Site Greifswald, Fleischmannstr. 42, 17489 Greifswald, Germany

[4]Biomedical Engineering Division, James Watt School of Engineering, University of Glasgow, G12 8LT

Supplementary Figures

Cell type/ process	Channel specifications	Process specifications	Ref.
Cell cycle synchronisation of several cell lines (HeLa, KKU-100, CHO-CD36 and hMSCs)	Spiral channel (9 loops, 40cm long, single inlet, 8 outlets) 500µm wide Height was fine tuned for each cell type to satisfy $a/D_h>0.07$ Made of PDMS	Throughput: 15×10^6 cells/h Flow rate: 2.5ml/min Enrichments of cells at G0/G1: >85% Viability: 95%	1
Focusing and ordering of HL-60 and K562 cells to facilitate deterministic single cell encapsulation in droplets	Spiral channel (5 loops, 7.2cm long), 50µm wide, 29µm high, initial radius of 1500µm Made of PDMS	Flow rate: 15µl/min	2
Separation of tumour cells (MCF-7 and HeLa) from spiked blood sample	Double spiral channel (12 loops: 6 loops counter-clockwise & 6 loops clockwise, one inlet, three outlets), 300µm wide, 50µm deep Made of PDMS	Throughput: 3.33×10^7 cells/min Flow rate: 350µl/min Recovery: 88.5%	3
Isolation of CTC from whole diluted blood (20-25% hematocrit) from	Spiral channel (2 loops, 10cm long, 2 inlets, 2 outlets), 500µm wide, 160µm deep	Flow rate: 3ml/hr Efficiency: 88% Detection rate: 100% (cells	4

cancer patients.	Made of PDMS	detected in all cancer patients' blood samples, n=20)	
Separation of single cells from cell clumps for murine neurosphere assay	Spiral channel (5 loops, one inlet, 8 outlets), 500µm wide, 150µm deep, initial radius of curvature 1cm. Made of PDMS	Efficiency: 75% Flow rate: 3ml/min Viability: >97%	5
Separation of plasma from whole blood sample ×20 diluted	Spiral channel (5 loops, 16cm long, one inlet, two outlets), 150µm wide, 50µm deep, the initial radius was 3500µm. Made of PDMS	Throughput: 700µl/min Efficiency: 38.5% Plasma purity: 99.9%	6
Separation of non-motile sperm cells from RBC in TESE/mTESE samples	Spiral channel (4 loops, 1 inlet, 4 outlets), 150µm wide, 50µm deep, the initial radius was 700µm Made of PDMS	Throughput: 520µl/min Efficiency: 81% for sperm cells, 99% for RBC	7
Separation of higher quality sperm from lower quality sperm without using sperm motility	Spiral channel (4 loops, 1 inlet, 4 outlets), 150µm wide, 50µm deep, initial radius 853µm. Made of PDMS	Throughput: 550µl/min Cell concentration:2×10^7 cells/ml Higher quality sperm was 4 times enriched in comparison to the input	8
Separation and concentration of *Phytopthora ramorum* sporangia (fungal plant phatogen, Ø30µm)	Spiral channel (3 loops, 1 inlet, 2 outlets), 600µm wide, 200µm deep, the radius of curvature was 2cm on average Made of thermoplastic polymer	Throughput: 2ml/min 5.3-fold increase in pathogen content with 95% recovery	9
Separation of algae (sub-millimetre phytoplankton) of two specimens: *Monoraphium griffithii* from *Cyanothece aeruginosa.*	Spiral channel (3 loops, 1 inlet, 2 outlets), 350µm wide and 100µm deep, initial radius 5mm, total length ~14cm Made of PDMS	Flow rate: 3.2ml/min Efficiency: 77%	10
Isolation of blood plasma, blood sample diluted 1:20	A cascade of two spiral channels, each with 1 inlet,3 outlets and 5 loops: 1st: 500µm wide, 60µm deep 2nd: 250µm wide, 60µm deep Made of PDMS	Flow rate: f 1.25ml/min Efficiency: 1st: 55% of blood cells removed 2nd: 99% of blood cells removed	11
Concentration of *E.coli* and 1µm beads	Spiral channels (3 loops, 1 inlet and 2 outlets): 1st part : 10 × 24µm^2 cross-section	Flow rate: 50µl/min (generated 70 bars) 100µl/min (generated 150	12

	2nd part: 10 × 60µm² cross-section Made of glass to withstand high pressure (up to 200 bar)	bars)	
Separation of neural stem cells derived from induced pluripotent stem cells from spontaneously differentiated non-neural cells	Spiral channel (1 inlet, 8 outlets and 10 loops), 500µm wide and 160µm deep, total length ~ 50cm Made of PDMS	Flow rate: 3ml/min Efficiency: 2.5× enrichment of neural stem cells with 38% recovery	[13]
Enrichment of mesenchymal stem cells from bone marrow	Spiral channel (1 inlet, 8 outlets, 10 loops), 500µm wide and 160µm deep, total length ~50cm	Flow rate: up to 3 ml/min Efficiency: the best performance at 1.6ml/min, 6× enriched, 73% recovery rate	[14]

STable. 1
Examples of published data using IF in spiral channels with a symmetrical cross-section for size-based separating a wide range of biological samples.

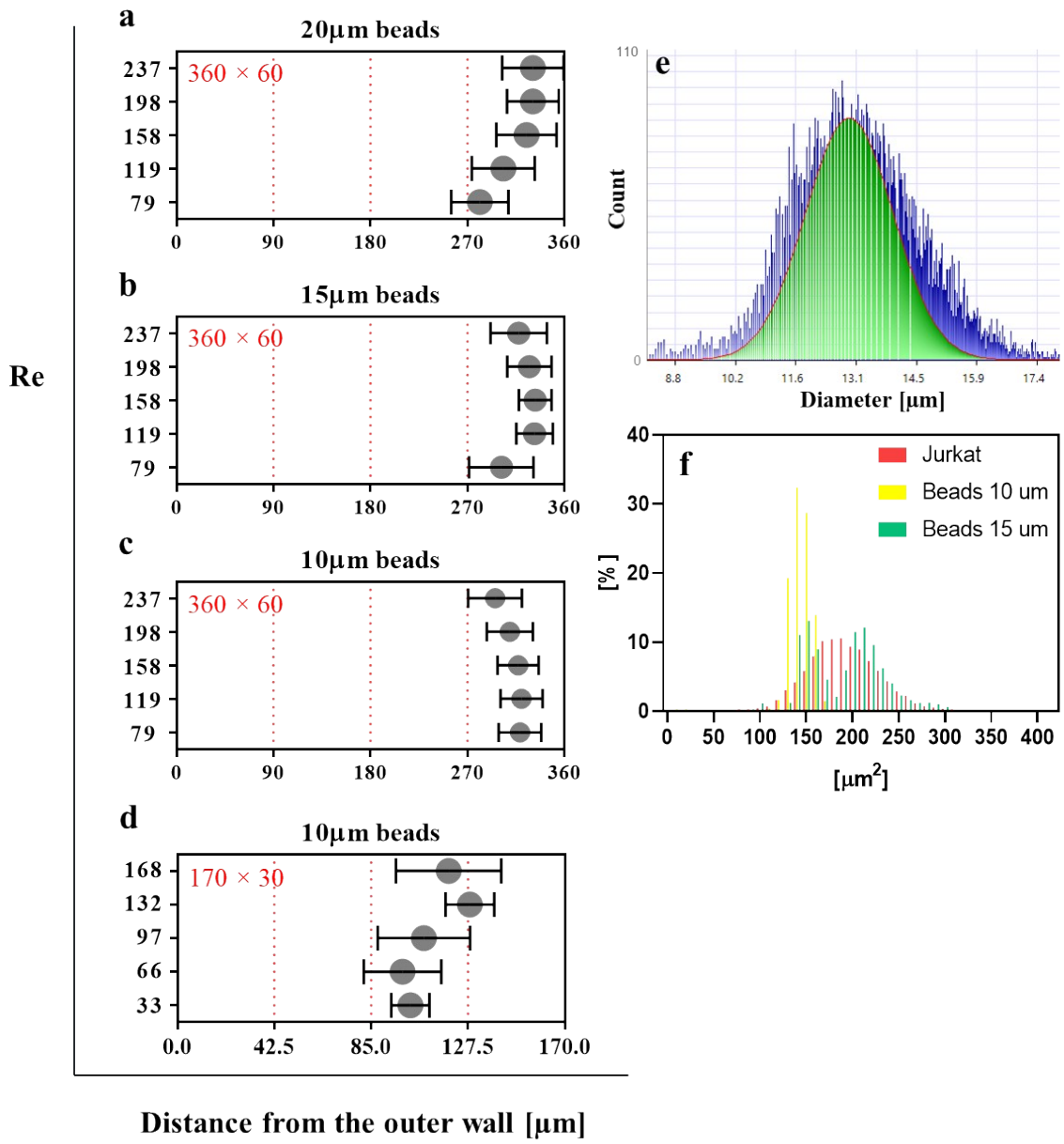

SFig.1

Hydrodynamic behaviour of polystyrene beads with **(a)** 20, **(b)** 15 and **(c)** 10, µm diameter in design I spiral microchannel with 360 × 60 µm^2 cross-section at five different flow rates corresponding to Re=79, 119, 158, 198 and 237 and **(d)** 10 µm diameter in design II spiral microchannel with 170 × 30 µm^2 cross-section, at five different flow rates corresponding to Re=33, 66, 97, 132 and 168. The lateral equilibrium positions were measured as a distance from the outer wall (µm) at the end of the spiral channel for at least 10000 events and there were generated by image analysis. Here, it is reported as mean (represented as the symbols) and standard deviation (indicated by the short vertical lines). Vertical dotted lines indicate four sections of the channel corresponding to four outlets of the channel (0-90 µm- outlet A, 90-180 µm- outlet B, etc.). Events belonging to a given section have the highest probability of being captured within the corresponding outlet. **(e)** Size measurement report generated for Jurkat cells using MoxiZ automated cell counter. The report is a histogram, where blue vertical lines

indicate number of cells measured within a given size range (bins), the red curve is a fit into the data generated automatically by the MoxiZ software and green color indicated area under the curve. **(f)** A histogram showing percentage of size ranges found within Jurkat cells population (red) in comparison to 10 (yellow) and 15 (green) µm beads. Please note that there are discrepancies in sizes measured with the MoxiZ and by the image analysis. MoxiZ measures light scatter around the measured particles which is further converted by an algorithm into a numerical value, while size measured by image analysis is reported as a projected particle's area.

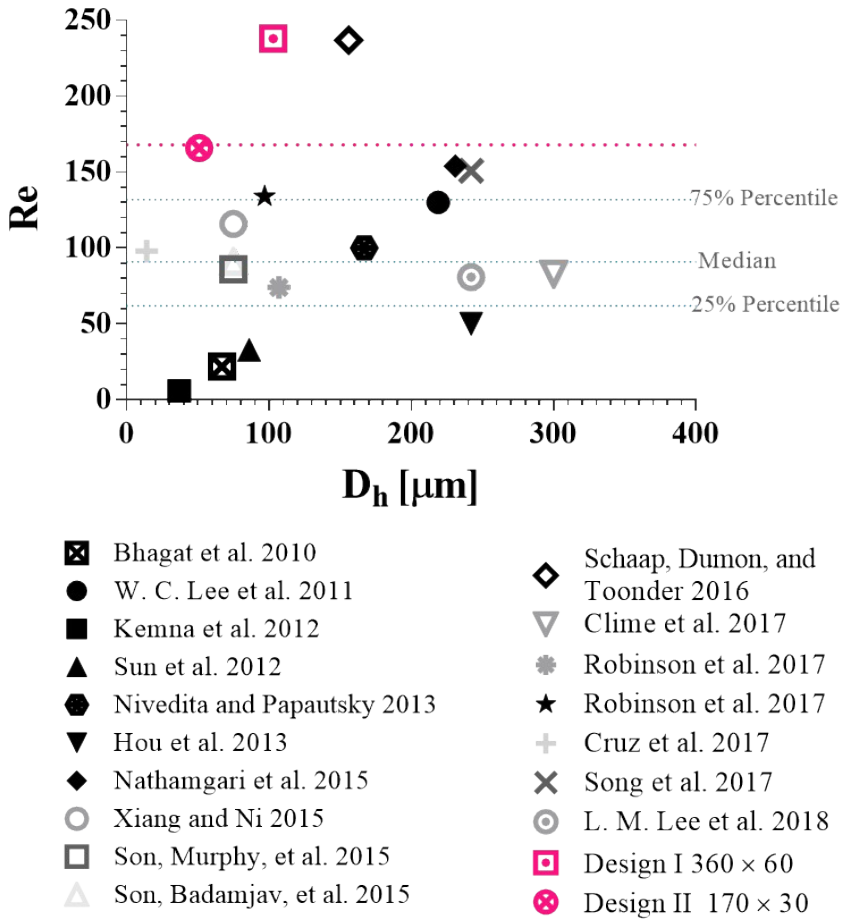

SFig. 3

Summary of operating conditions of spiral channels reported in the literature, up to end of 2018, in comparison to design I and II (pink). The scatter plot represents applied Re numbers versus hydraulic diameter (D_h). The grey dotted lines represent median Re number value (excluding design I and II) and lower and upper quartile as labelled on the graph. The pink dotted line represents the Re number applied in design II at which the effect of F_D was significant.

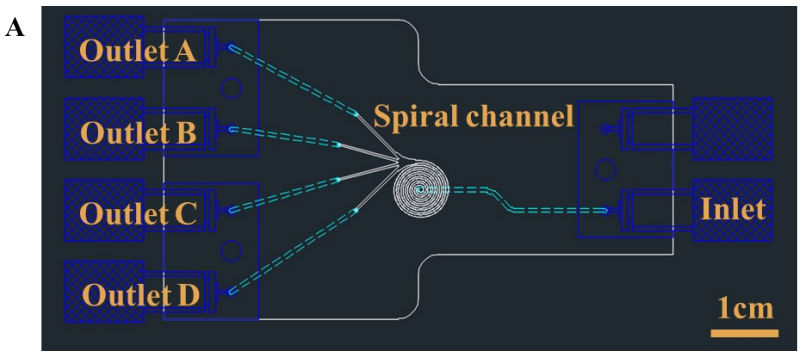

SFig. 4
(A) *Schematic of the spiral channel with six loops, one inlet and four outlets for size and deformability-based separation. Scale bar corresponds to 1 cm.*

	Flow rate [ml/min]	Velocity [m/s]	Re [-]	De
Design I	1	0.8	79	18
	1.5	1.2	119	27
	2	1.5	158	35
	2.5	1.9	198	44
	3	2.3	237	53
Design II	0.2	0.65	33	5
	0.4	1.3	66	10
	0.6	1.9	97	15
	0.8	2.6	132	21
	1	3.3	168	26

STable 2
Table summarising experimental conditions (applied flow rates and corresponding velocities, Reynolds numbers (Re) and Dean numbers (De)) in design I (with 360 × 60 µm² cross section) and design II (with 170 × 30 µm² cross-section).
De is used to quantify the secondary flow within spiral microchannel, and it is defined as $De = Re\sqrt{\frac{D_h}{R}}$*, where Dh is hydraulic diameter, for channles with rectangular cross section defined as* $D_h = \frac{2 \times H \times W}{H + W}$*, where H- channel height and W- channel width.*

Supplementary materials and methods

Real-time fluorescence and deformability cytometry

While there are many available well-established technologies for assessing cell mechanotype such as Atomic Force Microscopy (AFM) [15], micropipette aspiration [16], magnetic tweezers and optical stretchers [17], these methods suffer from low-throughput [18]. To assess a high number of cells (thousands of events per minute), we used a microfluidic-based Real-Time Deformability Cytometer (RT-DC) [19]. RT-DC is a contactless technique, allowing gain of thousands of events per minute, which is convenient for the global characterisation of complex samples [20]. In the RT-DC set-up, a PDMS (Polydimethylsiloxane) channel consisting of three sections, two reservoir sections and one constriction channel (20 μm × 20 μm or 30 μm × 30 μm cross section), where cells undergo deformation and measurements are undertaken. The microfluidic chip is mounted on a microscope. A syringe pump is used to pump cells suspension in the chip, pulsing LED light enables high-speed image acquisition (4000 fps), for a standard measurements, the images are acquired at 40x magnification. Cells are introduced in the chip through central reservoir channel and they are directed into the measurement channel by sheath flow (both flow liquid and cell carrier are viscous solution of methylcellulose). Measurement channel has a cross-section slightly bigger than the cell diameter, thus cells entering the channel experiences shear stress that causes cell deformation. The images are captured in the Region of Interest (ROI) at the end of the measurement channel and processed in real time.

The RT-DC system employs image processing algorithms which enable the measurement of cell area and deformation. Deformation (D) is expressed as a deviation from a perfect circle

$$D = 1 - c \tag{1}$$

where c is the circularity defined as

$$c = 2\sqrt{\pi A}/l \tag{2}$$

A being the projected cell area and l the cell perimeter

Deformation (D) in the channel is independently measured from the initial cell shape and therefore any treatment-induced morphological changes to shape. Consequently, when possible, a differential deformation DD parameter has been introduced [21].

DD includes morphological information acquired in the reservoir (D_{Res})section of the RT-DC chip (where applied shear is negligible) by subtracting this value from the deformation measured in the channel (D_{Ch}). From each vector of deformations values with length n, sampling is done with replacement n-times and the resulting distribution is used to calculate a statistic like the median (M). A single DD value is computed using

$$DD_{j,CH} = D_{j,Ch} - D_{j,Res} \quad (3)$$

Subtraction is done by statistical representations of channel and reservoir measurements and using a bootstrapping approach. The process of sampling, calculation of M and DDj has to be repeated for a sufficient number of iterations (>1000) to obtain a bootstrap distribution follows a Gaussian distribution [21,22].

RT-FDC is an enhanced high-throughput (thousands of events per minute) microfluidic platform that enables mechanotype analysis of cells within a heterogeneous sample with no necessity of pre-sorting into pure populations, due to the integration of fluorescent signal for confirmation of cell identity [23]. As in the conventional real-time deformability cytometry (RT-DC) [19], cells are deformed in a contactless manner by experiencing shear stress generated by flowing in a viscous buffer through the measurement channel which is only slightly larger than the actual cell dimensions. In RT-FDC **(1)** Immuno-labelled cells are introduced into the microfluidic chip mounted on a microscope and while passing through the measurement channel **(2)** in the ROI they are imaged by bright-field microscopy **(3)**. Information about cells size (expressed as projected cell area [μm^2]) and induced by applied shear stress deformability (understood as 1- circularity) is generated by image processing in real time for each captured event and reported as a scatter plot. Additionally, cells passing through the ROI are illuminated by focused lasers **(4)** which excite signal detected and measured in the detector array. **(5)** The fluorescent signal is correlated with the acquired image, which allows cell identity confirmation.

Summary of Triplicate results

The hydrodynamic behaviour of cells was assessed in terms of lateral equilibrium position (measured as a distance from the particle centre to the outer wall [µm]) obtained at the end of the spiral channel by monitoring the ROI, by high-speed microscopic imaging. For one replica of one condition at one flow rate we obtained at least 10000 events. As an example, we provide **SFig. 5** showing a single image extracted from a video recorded for soft cells at flow rate corresponding to Re=119 in the spiral channel with 360 × 60 µm^2 cross-section. All of the raw files can be accessed upon a request.

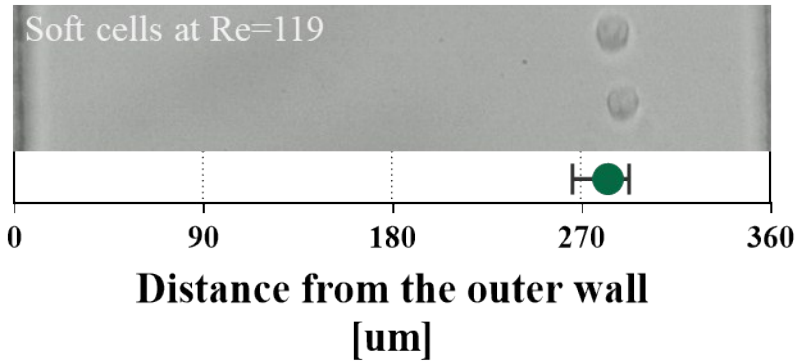

SFig. 5
An exemplary image extracted from a video recorded for soft cells at flow rate corresponding to Re=119 in the spiral channel with 360 × 60 µm^2 cross-section. in comparison to the statistical summary of the lateral equilibrium position (expressed as distance from the pouter wall [µm]) reported as median (represented as the symbol) and the interquartile range (indicated by the short vertical lines). Vertical dotted lines indicate four sections of the channel corresponding to four outlets of the channel (0-90 µm- outlet A, etc.).

Design I: Hydrodynamic behaviour of cells of cellular deformability model

Hydrodynamic behaviour of cells (10000 per condition) of five different deformabilities (soft max, soft half-max, soft, stiff half-max and stiff) (A) in comparison to reference 15 µm beads in design I spiral microchannele with 360 × 60 µm^2 cross-section at five different flow rates corresponding to Re=79, 119, 158, 198 and 237 The lateral equilibrium positions were measured as a distance from the outer wall (µm) at the end of the spiral channel and there were generated by image analysis. Here, it is reported as median (represented as the symbols) and the interquartile range (indicated by the short vertical lines). Vertical dotted lines indicate four sections of the channel corresponding to four outlets of the channel (0-90. µm- outlet A, 90-180 µm- outlet B, etc.). Events belonging to a given section have the highest probability of being captured within the corresponding outlet **and** tables showing statistical summary (mean and standard deviation from the mean (SD), median, 25th (Qi) and 75th (Q3) percentile as well as minimal (min) and maximal (max) measured value) of latera equilibrium positions obtained for at least 10000 events.

Design I: Hydrodynamic behaviour of cells of cellular deformability model

Replica I

Re=237

Re=237	Mean	SD	Min	Q1	Median	Q3	Max
Soft max	122	49	37	86	112	144	328
Soft half-max	110	44	33	79	101	131	334
Soft	132	50	38	98	124	156	335
Stiff half-max	251	77	34	191	289	308	338
Stiff max	305	45	33	304	316	331	341
15µm beads	318	26	43	308	328	335	339

Re=198

Re=198	Mean	SD	Min	Q1	Median	Q3	Max
Soft max	201	66	46	150	198	261	335
Soft half-max	169	59	36	127	161	205	335
Soft	203	62	46	155	201	256	337
Stiff half-max	270	62	20	254	294	308	338
Stiff max	310	29	63	303	313	327	339
15µm beads	328	21	34	325	337	337	340

Re=158

Re=158	Mean	SD	Min	Q1	Median	Q3	Max
Soft max	265	51	48	248	285	298	336
Soft half-max	242	57	43	206	262	286	335
Soft	265	46	47	251	282	295	337
Stiff half-max	273	51	49	263	289	302	338
Stiff max	306	24	61	299	308	318	338
15µm beads	333	15	80	337	338	338	341

Re=119

Re=119	Mean	SD	Min	Q1	Median	Q3	Max
Soft max	281	34	69	276	291	301	335
Soft half-max	269	39	16	259	281	292	334
Soft	273	33	40	266	283	293	335
Stiff half-max	268	42	71	259	281	292	336
Stiff max	294	24	67	287	297	306	337
15µm beads	332	17	46	336	337	338	341

Re=79

Re=79	Mean	SD	Min	Q1	Median	Q3	Max
15µm beads	302	30	8	295	303	317	337
Stiff max	270	27	35	264	277	286	334
Stiff half-max	259	36	49	249	270	281	332
Soft	265	29	90	259	274	283	335
Soft half-max	263	34	18	255	273	283	332
Soft max	273	32	20	265	282	292	334

Distance from the outer wall [um]

Design I: Hydrodynamic behaviour of cells of cellular deformability model

Replica II

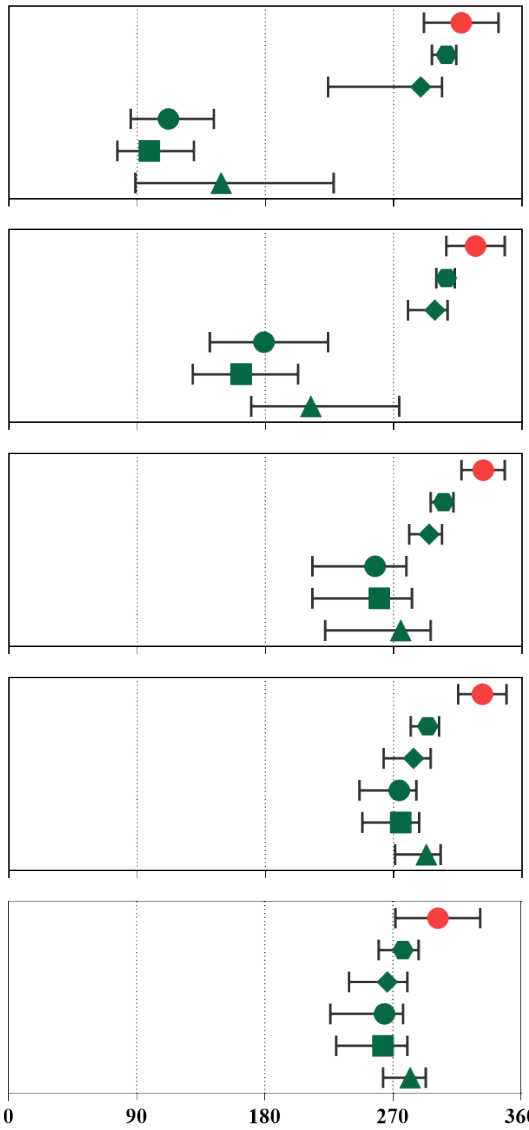

Re=237	Mean	SD	Min	Q1	Median	Q3	Max
15µm beads	318	26	43	308	328	335	339
Stiff max	298	34	67	297	307	314	337
Stiff half-max	258	67	22	224	289	304	339
Soft	123	53	36	86	112	144	336
Soft half-max	111	50	35	76	99	130	336
Soft max	168	87	47	89	149	228	335

Re=198	Mean	SD	Min	Q1	Median	Q3	Max
15µm beads	328	21	34	325	337	337	340
Stiff max	304	21	102	300	307	313	335
Stiff half-max	280	52	49	280	299	308	338
Soft	184	60	34	141	179	224	337
Soft half-max	169	57	37	129	163	203	336
Soft max	219	60	60	170	212	274	337

Re=158	Mean	SD	Min	Q1	Median	Q3	Max
15µm beads	333	15	80	337	338	338	341
Stiff max	301	23	83	296	305	312	336
Stiff half-max	284	39	52	281	295	304	337
Soft	242	48	53	213	257	279	337
Soft half-max	244	51	50	213	260	283	336
Soft max	255	54	62	222	275	296	335

Re=119	Mean	SD	Min	Q1	Median	Q3	Max
15µm beads	332	17	46	336	337	338	341
Stiff max	287	28	67	282	294	302	337
Stiff half-max	273	38	51	263	284	296	337
Soft	261	37	71	246	274	286	336
Soft half-max	263	37	17	248	275	288	334
Soft max	280	37	51	271	293	303	337

Re=79	Mean	SD	Min	Q1	Median	Q3	Max
15µm beads	302	30	8	295	303	317	337
Stiff max	269	30	78	260	277	288	335
Stiff half-max	254	38	65	239	266	280	324
Soft	250	38	41	226	264	277	325
Soft half-max	252	37	20	230	263	280	335
Soft max	274	30	52	263	282	293	336

Design I: Hydrodynamic behaviour of cells of cellular deformability model

Replica III

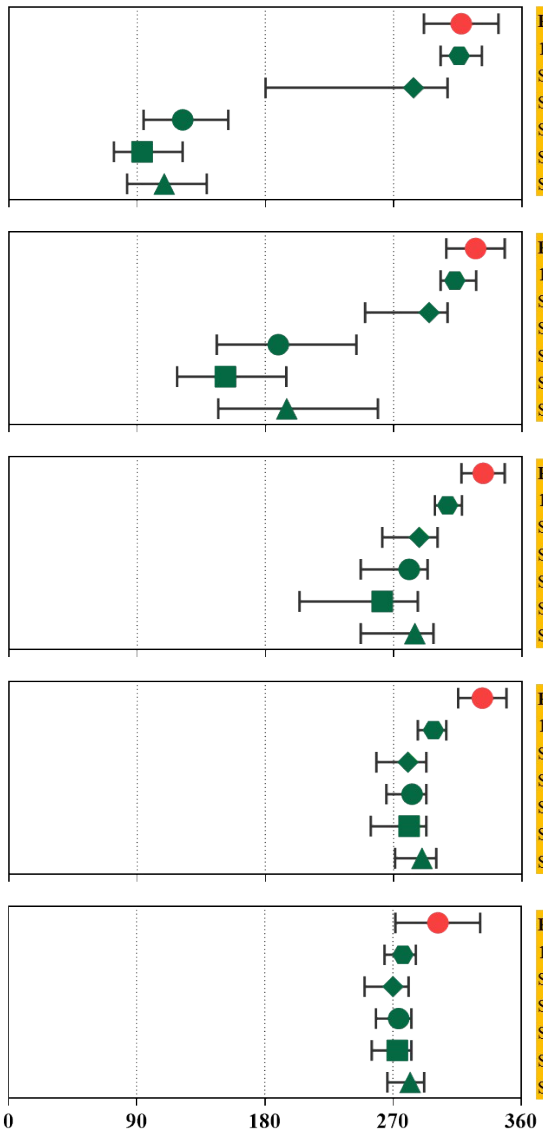

Re=237	Mean	SD	Min	Q1	Median	Q3	Max
15µm beads	318	26	43	308	328	335	339
Stiff max	304	47	49	303	316	332	341
Stiff half-max	246	79	30	180	284	308	339
Soft	131	51	43	95	122	154	336
Soft half-max	105	45	36	74	94	122	335
Soft max	119	49	35	83	109	139	332

Re=198	Mean	SD	Min	Q1	Median	Q3	Max
15µm beads	328	21	34	325	337	337	340
Stiff max	310	30	12	303	313	328	340
Stiff half-max	269	64	34	250	295	308	338
Soft	194	63	47	146	189	244	337
Soft half-max	161	61	18	118	152	195	334
Soft max	198	66	41	147	195	259	336

Re=158	Mean	SD	Min	Q1	Median	Q3	Max
15µm beads	333	15	80	337	338	338	341
Stiff max	307	23	79	299	308	318	338
Stiff half-max	273	50	59	262	288	301	337
Soft	264	47	51	247	281	294	337
Soft half-max	242	58	18	204	262	287	336
Soft max	264	52	43	247	285	298	335

Re=119	Mean	SD	Min	Q1	Median	Q3	Max
15µm beads	332	17	46	336	337	338	341
Stiff max	295	25	75	287	298	307	337
Stiff half-max	267	43	53	258	280	293	336
Soft	272	34	82	265	283	293	337
Soft half-max	266	42	18	254	281	293	334
Soft max	277	40	21	271	290	300	335

Re=79	Mean	SD	Min	Q1	Median	Q3	Max
15µm beads	302	30	8	295	303	317	337
Stiff max	271	27	52	264	277	286	333
Stiff half-max	259	35	60	250	270	281	332
Soft	265	29	94	258	274	283	334
Soft half-max	262	34	19	255	273	283	330
Soft max	274	32	22	266	282	292	335

Design II: Hydrodynamic behaviour of cells of cellular deformability model

Hydrodynamic behaviour of cells of five different degrees of deformability (Soft max, soft half-max, soft, stiff half-max and stiff) in comparison to reference 15 μm beads, in design II spiral channel with 170 × 30 μm cross-section at five different flow rates corresponding to Re=33, 66, 97, 132 and 168 (as outlined in the tables on the right) . The lateral equilibrium positions were measured as a distance from the outer wall (μm) at the end of the spiral channel and there were generated by image analysis. Here, it is reported as median (represented as the symbols) and the interquartile range (indicated by the short vertical lines). Vertical dotted lines indicate four sections of the channel corresponding to four outlets of the channel (0-90. μm- outlet A, 90-180 μm- outlet B, etc.). Events belonging to a given section have the highest probability of being captured within the corresponding outlet **and** tables showing statistical summary (mean and standard deviation from the mean (SD), median, 25^{th} (Qi) and 75^{th} (Q3) percentile as well as minimal (min) and maximal (max) measured value) of latera equilibrium positions obtained for at least 10000 events

Design II: Hydrodynamic behaviour of cells of cellular deformability model

Replica I

Re=168

Re=168	Mean	SD	Min	Q1	Median	Q3	Max
10µm beads	119	23	7	95	136	139	155
Stiff max	113	21	34	102	121	128	143
Stiff half-max	100	27	21	78	109	124	143
Soft	68	21	20	54	62	79	161
Soft half-max	80	26	20	59	74	96	142
Soft max	75	24	19	57	70	92	142

Re=132

Re=132	Mean	SD	Min	Q1	Median	Q3	Max
10µm beads	128	11	28	121	132	137	161
Stiff max	101	25	29	84	107	123	147
Stiff half-max	88	29	26	67	85	119	143
Soft	75	18	23	63	74	86	141
Soft half-max	84	23	20	66	83	102	143
Soft max	80	23	15	62	77	97	162

Re=97

Re=97	Mean	SD	Min	Q1	Median	Q3	Max
10µm beads	108	20	29	91	97	131	158
Stiff max	89	25	25	76	87	107	144
Stiff half-max	79	24	21	64	79	92	148
Soft	85	20	24	70	85	99	141
Soft half-max	85	20	24	70	85	99	141
Soft max	82	21	20	66	81	97	141

Re=66

Re=66	Mean	SD	Min	Q1	Median	Q3	Max
10µm beads	99	17	60	80	107	115	150
Stiff max	82	26	18	70	84	94	145
Stiff half-max	80	21	18	75	83	89	148
Soft	78	18	21	69	80	87	149
Soft half-max	84	18	19	74	85	96	144
Soft max	82	18	21	71	83	93	138

Re=33

Re=33	Mean	SD	Min	Q1	Median	Q3	Max
10µm beads	102	8	40	97	102	105	152
Stiff max	87	19	18	80	90	97	150
Stiff half-max	84	18	17	78	87	94	150
Soft	82	17	19	74	83	90	149
Soft half-max	86	19	18	77	89	98	148
Soft max	84	20	17	73	86	96	150

Distance from the outer wall [um]

Design II: Hydrodynamic behaviour of cells of cellular deformability model

Replica II

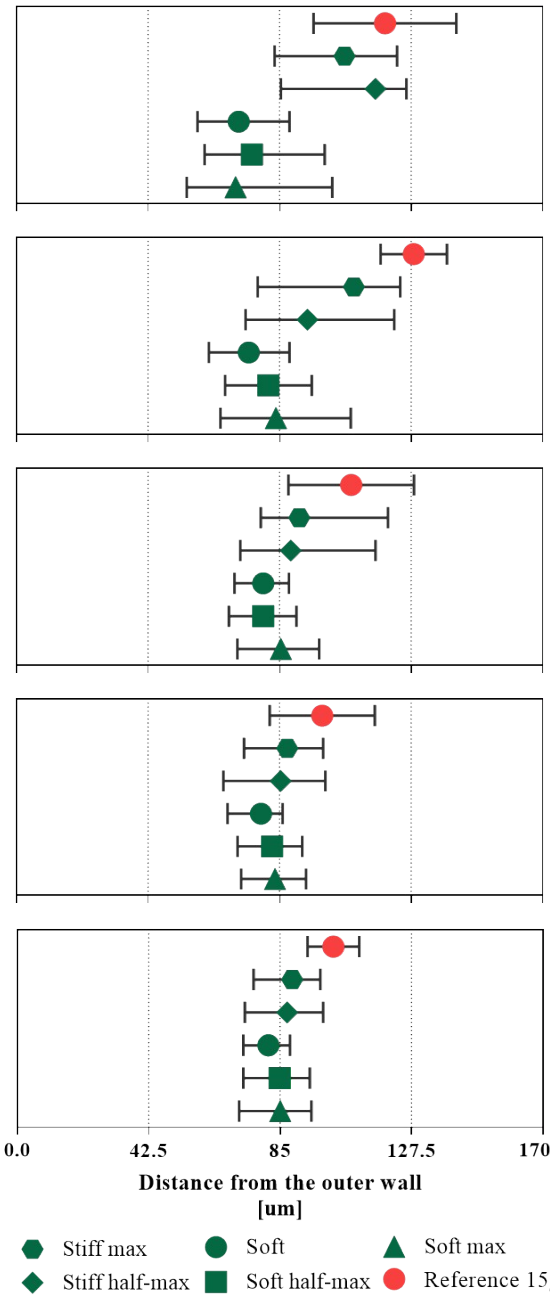

Re=168	Mean	SD	Min	Q1	Median	Q3	Max
10µm beads	119	23	7	95	136	139	155
Stiff max	101	26	21	83	106	123	142
Stiff half-max	104	27	30	85	116	126	143
Soft	75	23	15	59	72	88	145
Soft half-max	80	26	19	61	76	100	142
Soft max	78	28	25	55	71	102	138

Re=132	Mean	SD	Min	Q1	Median	Q3	Max
10µm beads	128	11	28	121	132	137	161
Stiff max	100	27	21	78	109	124	143
Stiff half-max	94	28	22	74	94	122	146
Soft	76	20	17	62	75	88	144
Soft half-max	82	20	17	67	81	95	137
Soft max	86	24	31	66	84	108	135

Re=97	Mean	SD	Min	Q1	Median	Q3	Max
10µm beads	108	20	29	91	97	131	158
Stiff max	94	26	21	79	91	120	155
Stiff half-max	90	28	27	72	89	116	144
Soft	80	15	21	70	80	88	145
Soft half-max	80	18	28	69	80	90	133
Soft max	85	19	30	71	85	98	141

Re=66	Mean	SD	Min	Q1	Median	Q3	Max
10µm beads	99	17	60	80	107	115	150
Stiff max	86	27	23	74	88	99	155
Stiff half-max	84	27	20	67	85	100	151
Soft	77	18	18	68	79	86	143
Soft half-max	82	19	27	71	83	92	142
Soft max	83	20	17	73	84	94	141

Re=33	Mean	SD	Min	Q1	Median	Q3	Max
10µm beads	102	8	40	97	102	105	152
Stiff max	86	22	20	76	89	98	155
Stiff half-max	86	21	18	74	87	99	150
Soft	80	16	16	73	81	88	149
Soft half-max	84	19	18	73	85	95	149
Soft max	83	21	16	72	85	95	152

Design II: Hydrodynamic behaviour of cells of cellular deformability model

Replica III

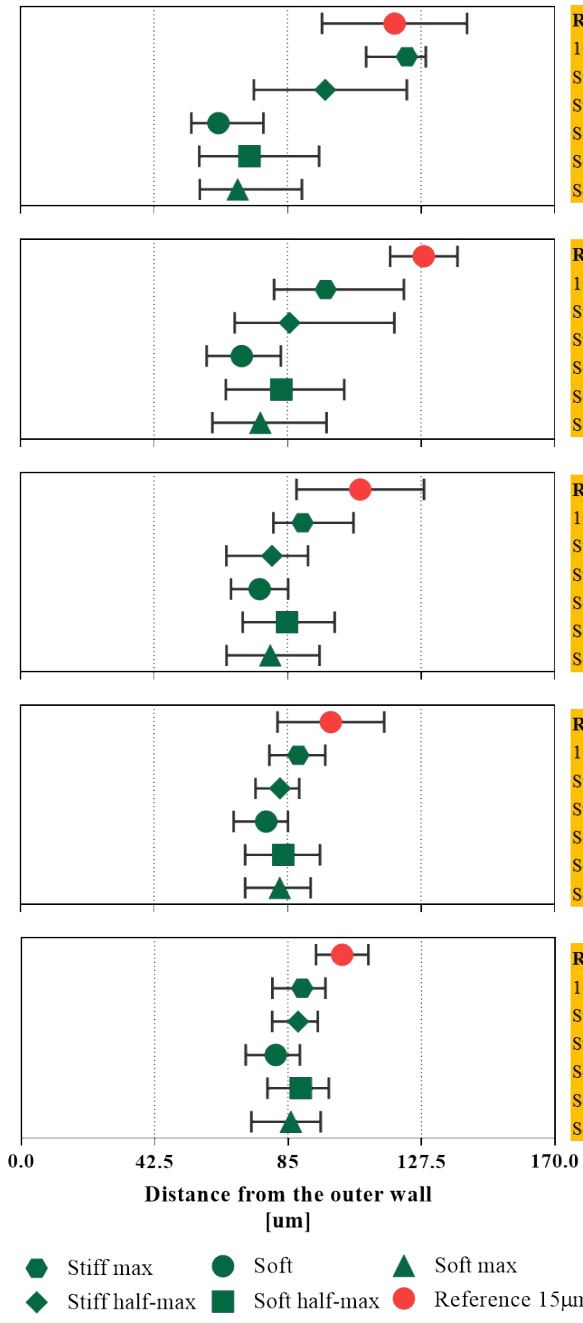

Re=168	Mean	SD	Min	Q1	Median	Q3	Max
10µm beads	119	23	7	95	136	139	155
Stiff max	115	21	31	110	123	129	155
Stiff half-max	96	28	28	74	97	123	143
Soft	68	21	23	54	63	77	145
Soft half-max	77	25	17	57	73	95	140
Soft max	74	23	19	57	69	90	140

Re=132	Mean	SD	Min	Q1	Median	Q3	Max
10µm beads	128	11	28	121	132	137	161
Stiff max	98	26	27	81	97	122	142
Stiff half-max	89	29	17	68	86	119	144
Soft	72	18	19	59	70	83	144
Soft half-max	84	23	26	65	83	103	146
Soft max	80	23	18	61	76	97	142

Re=97	Mean	SD	Min	Q1	Median	Q3	Max
10µm beads	108	20	29	91	97	131	158
Stiff max	92	23	27	81	90	106	149
Stiff half-max	80	26	21	66	80	92	142
Soft	76	16	20	67	76	85	140
Soft half-max	86	21	20	71	85	100	145
Soft max	81	21	26	66	80	95	143

Re=66	Mean	SD	Min	Q1	Median	Q3	Max
10µm beads	99	17	60	80	107	115	150
Stiff max	87	23	21	79	88	97	150
Stiff half-max	80	21	18	75	83	89	147
Soft	76	17	21	68	78	85	143
Soft half-max	83	19	23	72	84	95	141
Soft max	82	18	24	72	83	92	135

Re=33	Mean	SD	Min	Q1	Median	Q3	Max
10µm beads	102	8	40	97	102	105	152
Stiff max	87	19	18	80	90	97	149
Stiff half-max	85	17	17	80	88	95	148
Soft	80	18	15	72	81	89	147
Soft half-max	87	18	17	78	89	98	150
Soft max	84	20	14	73	86	95	151

Summary of flow cytometric viability assay. On the top- an exemplary scatter plot showing gating strategy for live cell (green, negative for both Alexa Fluor 488-annexin V and propidium iodide (PI) fluorescence), apoptotic cells (orange, annexin V-positive and PI-negative) and necrotic (red, annexin V-positive and PI-positive). Summary of flow cytometric assessment of the presence of live, apoptotic and necrotic Jurkat cells before (stained control and after processing (stained test).

Design I spiral channel with 360 × 60 µm cross-section at highest applied flow rate (Re=237) for three replicas.

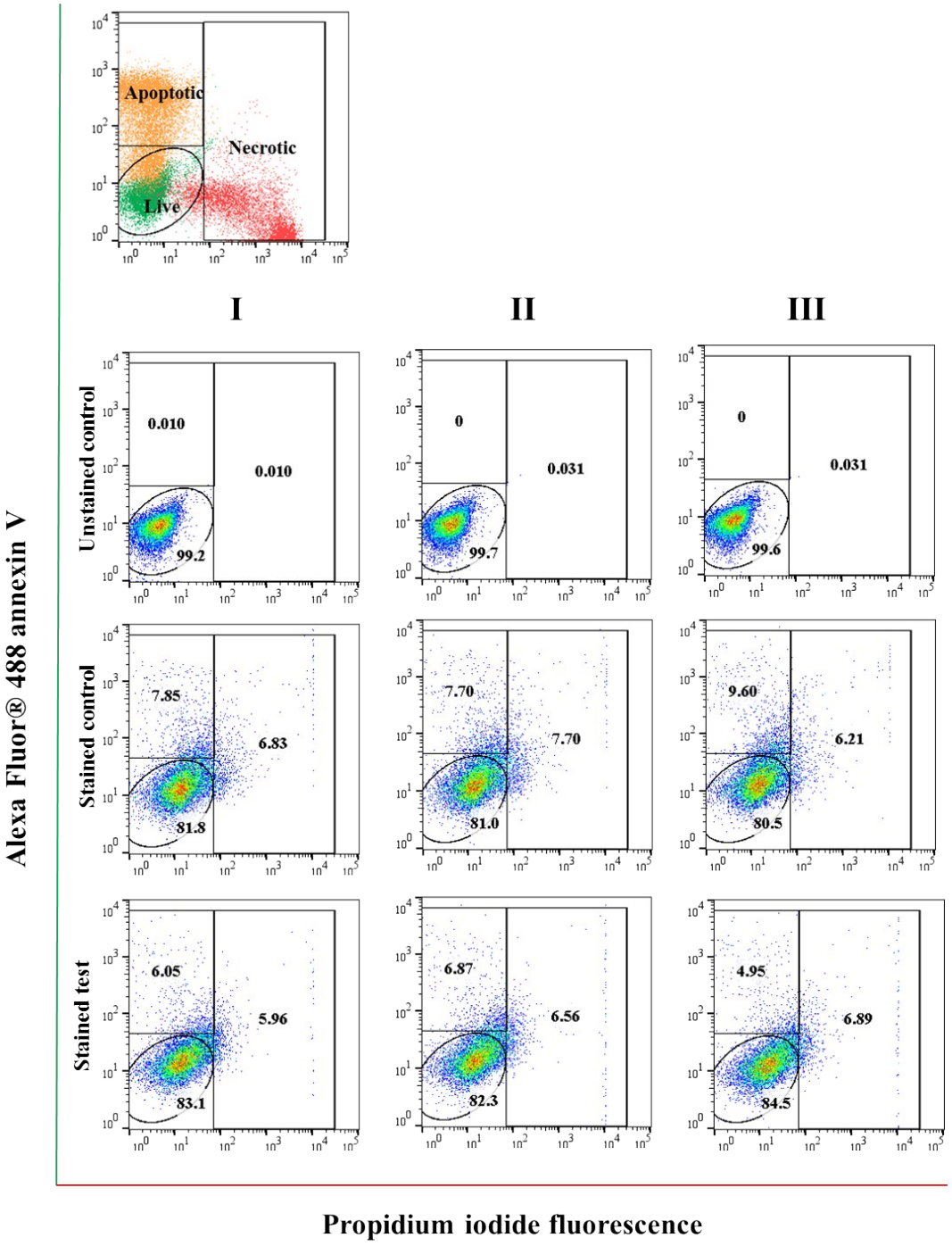

Design II spiral channel with 170 × 30 µm cross-section at highest applied flow rate (Re=168) for three replicas.

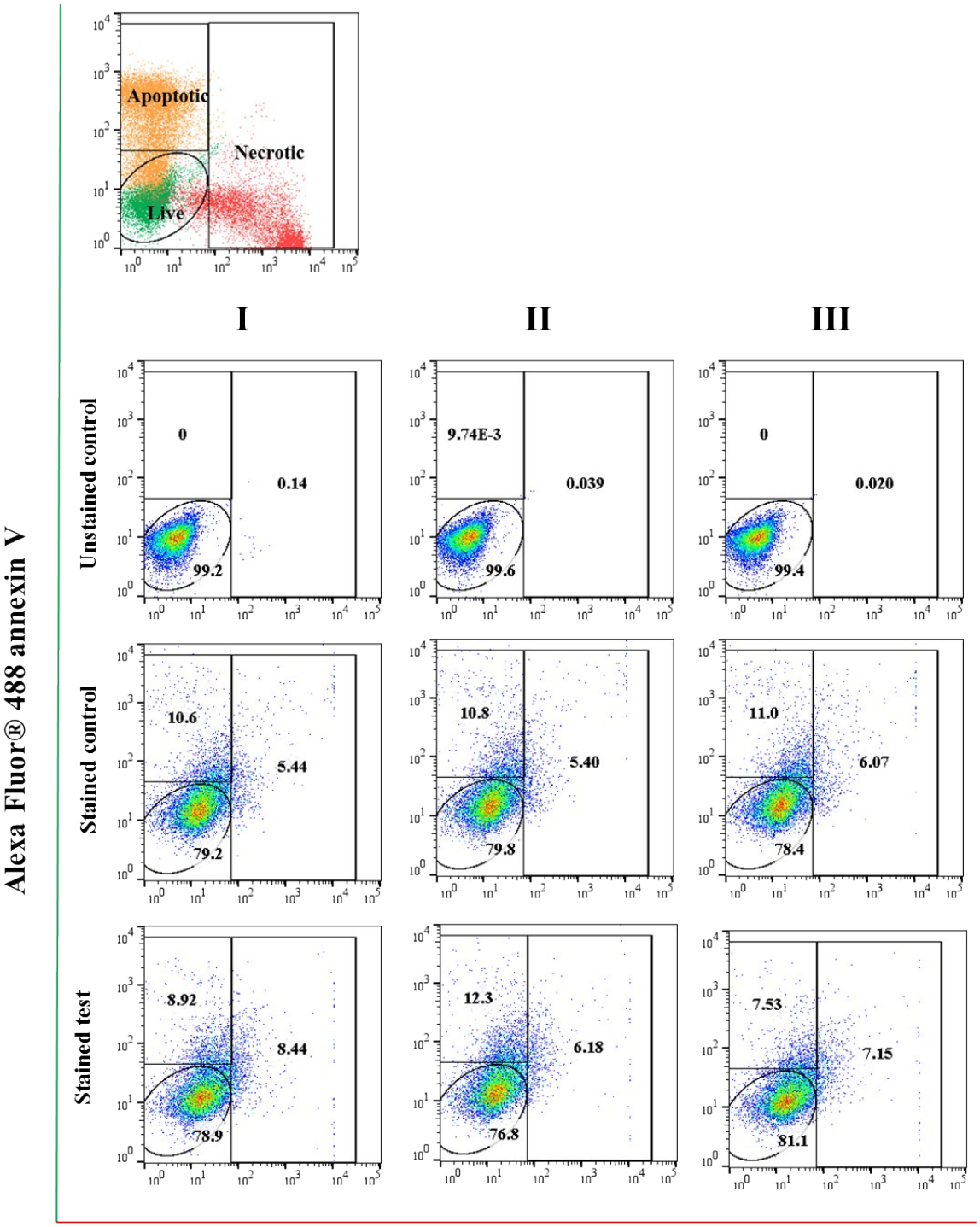

Bibliography

1. Lee, W. C. *et al.* High-throughput cell cycle synchronization using inertial forces in spiral microchannels. *Lab Chip* **11**, 1359–1367 (2011).
2. Kemna, E. W. M. *et al.* High-yield cell ordering and deterministic cell-in-droplet encapsulation using Dean flow in a curved microchannel. *Lab Chip* **12**, 2881–2887 (2012).
3. Sun, J. *et al.* Double spiral microchannel for label-free tumor cell separation and enrichment. *Lab Chip* **12**, 3952–3960 (2012).
4. Hou, H. W. *et al.* Isolation and retrieval of circulating tumor cells using centrifugal forces. *Sci. Rep.* **3**, 1–8 (2013).
5. Nathamgari, S. S. P. *et al.* Isolating single cells in a neurosphere assay using inertial microfluidics. *Lab Chip* **15**, 4591–4597 (2015).
6. Xiang, N. & Ni, Z. High-throughput blood cell focusing and plasma isolation using spiral inertial microfluidic devices. *Biomed. Microdevices* **17**, 1–11 (2015).
7. Son, J. *et al.* Non-motile sperm cell separation using a spiral channel. *Anal. Methods* **7**, 8041–8047 (2015).
8. Son, J. *et al.* Active Higher Quality Sperm Separation Using a Spiral Channel. in *19th International Conference on Miniaturized Systems for Chemistry and Life Science* 376–378 (2015).
9. Clime, L. *et al.* Separation and concentration of Phytophthora ramorum sporangia by inertial focusing in curving microfluidic flows. *Microfluid. Nanofluidics* **21**, 1–13 (2017).
10. Schaap, A., Dumon, J. & Toonder, J. den. Sorting algal cells by morphology in spiral microchannels using inertial microfluidics. *Microfluid. Nanofluidics* **20**, 1–11 (2016).
11. Robinson, M., Marks, H., Hinsdale, T., Maitland, K. & Coté, G. Rapid isolation of blood plasma using a cascaded inertial microfluidic device. *Biomicrofluidics* **11**, (2017).
12. Cruz, J. *et al.* High pressure inertial focusing for separating and concentrating bacteria at high throughput. *J. Micromechanics Microengineering* **27**, (2017).
13. Song, H. *et al.* Spiral-shaped inertial stem cell device for high-throughput enrichment of iPSC-derived neural stem cells. *Microfluid. Nanofluidics* **21**, 1–9 (2017).
14. Lee, L. M. *et al.* Label-free mesenchymal stem cell enrichment from bone marrow samples by inertial microfluidics. *Anal. Methods* **10**, 713–721 (2018).
15. Vahabi, S., Nazemi Salman, B. & Javanmard, A. Atomic force microscopy application in biological research: a review study. *Iran. J. Med. Sci.* **38**, 76–83 (2013).
16. Darling, E. M. *et al.* Mechanical properties and gene expression of chondrocytes on micropatterned substrates following dedifferentiation in monolayer. *Cell. Mol. Bioeng.* **2**, 395–404 (2009).

17. Guck, J. *et al.* The optical stretcher: a novel laser tool to micromanipulate cells. *Biophys. J.* **81**, 767–784 (2001).

18. Musielak, M. Red blood cell-deformability measurement: review of techniques. *Clin. Hemorheol. Microcirc.* **42**, 47–64 (2009).

19. Otto, O. *et al.* Real-time deformability cytometry: on-the-fly cell mechanical phenotyping. *Nat Meth* **12**, 199–202 (2015).

20. Xavier, M. *et al.* Mechanical phenotyping of primary human skeletal stem cells in heterogeneous populations by real-time deformability cytometry. *Integr. Biol. (Camb).* **8**, 616–623 (2016).

21. Herbig, M., Mietke, A., Müller, P. & Otto, O. Statistics for real-time deformability cytometry : clustering , dimensionality reduction and significance testing. *Biomicrofluidics* **042214**, 1–37 (2018).

22. Golfier, S. *et al.* High-throughput cell mechanical phenotyping for label-free titration assays of cytoskeletal modifications. *Cytoskeleton* **74**, 283–296 (2017).

23. Rosendahl, P. *et al.* Real-time fluorescence and deformability cytometry. *Nat. Methods* **15**, 355–358 (2018).